International Journal of GEOMATE, March, 2025 Vol.28, Issue 127, pp.112-120
ISSN: 2186-2982 (P), 2186-2990 (O), Japan, DOI: https://doi.org/10.21660/2025.127.g14267
Geotechnique, Construction Materials and Environment

PHASED-CONTROLLED ACTUATOR SYSTEM CAPABLE OF VISUAL INSPECTION INSIDE IRON STRUCTURES

Sota Abe[1] and *Hiroyuki Yaguchi[1]

[1] Faculty of Engineering, Tohoku Gakuin University, Japan

*Corresponding Author, Received: 19 Nov. 2024, Revised: 24 Dec. 2024, Accepted: 28 Dec. 2024

ABSTRACT: In Japan, the percentage of bridges over 50 years old is rapidly increasing. Some bridges are restricted to vehicular traffic due to damage and deterioration caused by aging. However, bridge inspection is extremely difficult due to the location of some sites. Although many types of inspection robots have been developed to ensure worker safety, inspection techniques for bridges have not been fully established. In this study, a phase-controlled electromagnetic vibration actuator with four orthogonally arranged vibration components is proposed for moving on complex iron structures such as bridges. A prototype actuator system, in which two sets of actuators are mounted for inspection and connected in parallel to control the direction of movement and improve propulsion characteristics, is developed. Tests confirm that two receivers, a video capture device, and a personal computer can be used to perform visual inspections inside an iron structure. The actuator system has a maximum traction force of 1.1 N. It can transmit inspection images wirelessly, allowing inspection inside structures over long distances. The actuator system can move in any direction by combining rotational and translational reciprocating movements. The operation of an industrially useful inspection device is thus established. The actuator system is capable of visual inspection of iron structures on flat surfaces but not on stepped surfaces. Furthermore, heavy objects, such as an automatic percussion device with a mass of 260 g, cannot be mounted on the actuator system. By improving the magnetic circuit of the vibration component, the movement characteristics of the actuator system can be improved.

Keywords: Actuator system, Phase control, Vibration, Translational and rotational movement, Visual inspection

1. INTRODUCTION

In Japan, the percentage of bridges that are more than 50 years old is rapidly increasing. Some bridges are restricted to vehicular traffic due to damage and deterioration caused by aging. Therefore, the inspection and maintenance of infrastructure, such as large bridges, is an important task. However, bridge inspection is extremely difficult due to the location of some sites. Various inspection robots have been developed to ensure worker safety.

Inspection robots can move on walls using mechanisms such as suction systems using permanent magnets [1, 2], attraction control systems using electromagnets [3], coupled models of permanent magnets and magnetic wheels [4, 5], vacuum systems using pumps [6-8], coupled models of suction cups and vibrations [9, 10], models using claw grippers [11-13] and models using roller [14, 15]. These inspection robots use a number of electromagnetic motors with good controllability as the driving source. However, robots [1-7, 10, 13-15] with built-in electromagnetic motors require reduction gears or other devices to be inserted between the motor and mechanical components. Therefore, built-in electromagnetic motors increase weight, which is disadvantageous for inspecting walls and ceiling surfaces. Based on the above, the previously proposed robots equipped with electromagnetic motors cannot be expected to improve movement characteristics. On the other hand, robots [8-9, 11-12] without electromagnetic motors have low propulsion characteristics and controllability difficulties.

Robots based on drone technology have been extensively developed [16, 17]. However, they are generally large and weigh more than 5 kg. Smaller drones have also been proposed, but they cannot carry heavy objects. Furthermore, wind gusts and thunderstorms affect the inspection performance of drones. For this reason, inspection techniques using drone technology have not yet been fully established. Attempts have been made to establish inspection techniques for bridges based on theoretical analysis [18-21], but verification using actual machines is needed.

Generally, vibration and noise are considered harmful in engineering, and vibration control is applied [22-24]. On the other hand, attempts to effectively utilize mechanical vibration are an interesting engineering problem with few practical examples. As one example of vibration use, the present authors previously proposed a phase-controlled actuator that can move on magnetic materials [25, 26]. This is achieved by orthogonally arranging multiple vibration components and combining mechanical resonance and friction. The prototype actuator is compact, lightweight, and controllable. However, although this actuator has excellent propulsion characteristics per unit weight,

its traction is low and heavy objects such as inspection systems have not been mounted on it. Furthermore, the actuator does not take into account the space required for the inspection system.

In this study, a phase-controlled actuator with four orthogonally arranged vibration components in a square acrylic frame is proposed to improve the propulsion characteristics and provide a mounting location for the inspection system. In addition, a prototype actuator system, in which actuators with identical characteristics are connected in parallel by a flexible silicone rubber material, is developed. Two inspection systems consisting of a small camera with a transmitter and a battery are attached to the actuator system. The actuator system is capable of translational and rotational movement. Tests on actual equipment verify that two receivers, a video capture device, and a personal computer allow visual inspection within iron structures.

A future task is to improve the propulsion characteristics. The magnetic circuit of the vibration component proposed by the authors [25] needs to be further improved. The actuator proposed in this paper can be applied to various industrial fields as a new device for driving robots.

2. RESEARCH SIGNIFICANCE

As mentioned above, the inspection of bridges is extremely difficult due to the location of some sites. Although many inspection robots have been developed to ensure worker safety, inspection technology based on such robots has not been established. The significance of this research is that the proposed actuator system, which is easy to operate, allows the visual inspection of iron structures. The actuator system can be used to establish inspection technology for large iron structures.

3. STRUCTURE OF PHASE-CONTROLLED ACTUATOR

In order to improve the propulsion characteristics and incorporate an inspection system, an actuator with multiple vibration components that act as the propulsion source was developed within an acrylic frame. Fig. 1 shows a schematic diagram of the actuator prototype developed in this study, in which four vibration components (A, B, C, and D) with identical characteristics are orthogonally arranged in a square acrylic frame (thickness: 5 mm, width: 10 mm, side length: 110 mm). The coil springs that make up the vibration components are made of stainless steel and have an outer diameter of 12 mm and a free length of 25 mm. The permanent magnet is a NdFeB magnet with a diameter of 12 mm and a height of 2.5 mm, magnetized in the height direction. The electromagnets were fabricated by winding a

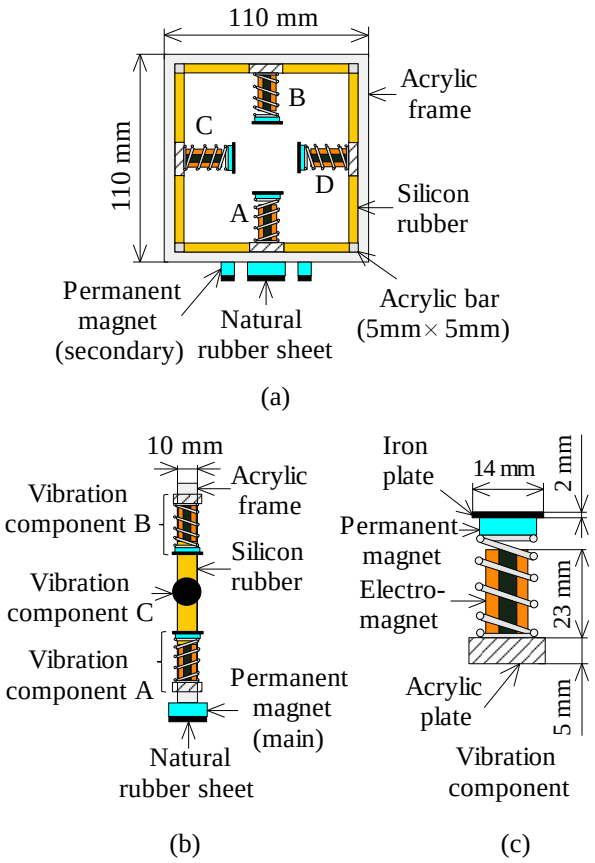

Fig. 1 Structure of actuator: (a) front view, (b) side view and (c) vibration component (cross section of center) of actuator

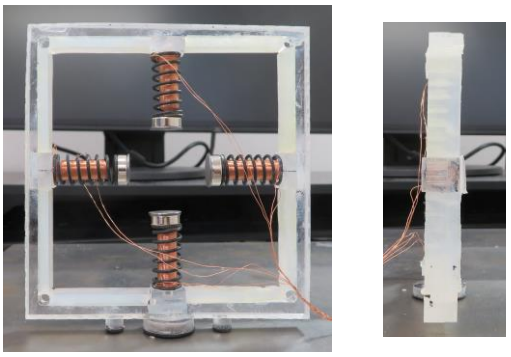

(a) (b)

Fig. 2 Photograph of actuator: (a) front view and (b) side view of prototype actuator

0.2-mm-diameter copper wire 840 times around a 3.8-mm-diameter iron core. The gap between the iron core and the permanent magnet is 5 mm in the stationary state. When prototyping the actuators, more than 10 vibration components were prototyped and only four vibration components with nearly identical characteristics were selected.

In order to reduce magnetic interference between the permanent magnets of the vibration components

mounted in the acrylic frame, an iron plate 14 mm in diameter and 2 mm thick was bonded to the permanent magnets, as shown in Fig. 1(c). This allows shielding of the magnetism between the permanent magnets. When an alternating current is applied to the electromagnets, electromagnetic excitation forces due to attraction and repulsion act on the permanent magnets, causing the vibration component to vibrate. In addition, to attract the actuator to the magnetic material, a main NdFeB magnet with an outer diameter of 20 mm and a thickness of 3 mm, magnetized in the height direction, and a natural rubber sheet with a thickness of 2 mm were bonded to the center of the acrylic frame to increase the frictional force, as shown in Figs. 1(a) and (b). A secondary permanent magnet with an outer diameter of 8 mm and a thickness of 1 mm was mounted 21 mm from the center of the frame to ensure stable linear movement of the actuator. The secondary permanent magnets were also bonded with a 2-mm-thick natural rubber sheet. The mounting positions of the secondary permanent magnets were determined from preliminary experiments.

When four vibration components were mounted in the corners of the acrylic frame, vibration interference caused by four components occurred. For the purpose of avoiding this effect, four vibration components were mounted in the center of the acrylic frame as shown in Fig. 1. The opposing vibration components (A/B and C/D) are vibrated as a set at the same frequency and phase. By controlling the phase difference between these components, the actuator can achieve reciprocating translational movement. In preliminary experiments, when two sets of vibration components placed opposite each other were driven at the same frequency, vibration interference occurred due to vibration waves propagating through the acrylic frame, which adversely affected the movement characteristics. To reduce this effect, eight pieces of flexible silicone rubber material, each 5 mm thick, 35 mm long, and 10 mm wide, were attached to the inside of the frame. The dimensions of the actuator

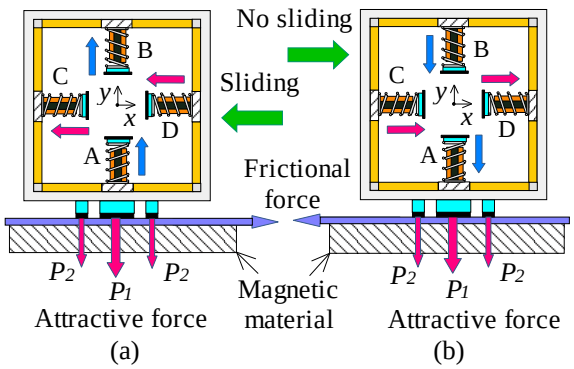

Fig. 3 Principle of locomotion : (a) sliding and (b) no sliding for locomotion of actuator

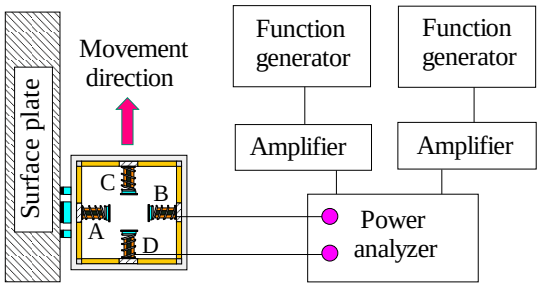

Fig. 4 Experimental apparatus

are 116 mm (height) × 110 mm (length) × 20 mm (width). The total mass *m* is 113 g. Fig. 2 shows a photograph of the prototype.

For the operation of vibration components A/B and C/D, the displacement coordinates *x* and *y* are defined as shown in Fig. 3 to illustrate the operating principle of the actuator. It is assumed that vibration components A and B and vibration components C and D vibrate in phase, respectively. As shown in Fig. 3, when the actuator is set on a magnetic material, the attractive force exerted by the main permanent magnet is P_1 and that exerted by the secondary permanent magnet is P_2. The attractive force P ($P_1 + 2P_2$) holds the actuator and allows the vibration component to vibrate.

As shown in Fig. 3(a), when vibration components A and B are displaced in the $+y$ direction, the friction force F_f decreases due to the force generated by the permanent magnets of vibration components A and B. When components C and D are displaced in the $-x$ direction, the actuator tends to slide in the $-x$ direction due to the force generated by the permanent magnets of vibration components C and D. On the other hand, as shown in Fig. 3(b), when the permanent magnets of vibration components A and B are displaced in the $-y$ direction, the friction force F_f increases due to the generated forces and the actuator does not move even when components C and D are displaced in the $+x$ direction. Therefore, the actuator can only move in the $-x$ direction. The direction of translational movement of the actuator can be switched by operating two sets of vibration components at the same frequency and setting the phase difference in vibration between the sets to 0 or 180 degrees.

4. MOVEMENT CHARACTERISTICS OF PHASE-CONTROLLED ACTUATOR

4.1 Experimental Setup

The movement characteristics of the prototype actuator were measured. Fig. 4 shows a schematic diagram of the experimental setup. An iron surface plate 300 mm wide, 300 mm long, and 60 mm thick was used as the magnetic material. A phase-controlled actuator was installed on the surface plate.

The actuator was driven by two two-channel signal generators and two amplifiers. The copper wires of the electromagnets in vibration components A/B and C/D were wired in parallel. Vibration components A/B and C/D were each connected to an amplifier so that they vibrated in phase. A digital stroboscope was used to confirm that the phase difference between the vibrations was 0 degrees. The input current and power to the electromagnets of the vibration components were measured using a two-channel power analyzer. The attractive force on the main permanent magnet to which the natural rubber sheet was attached was P_1 = 7.67 N and that on the secondary permanent magnet was P_2 = 1.26 N. The coefficient of friction between the natural rubber sheet and the surface plate was μ = 0.84. The driving frequency in each vibration component is 105 Hz.

4.2 Translational Movement Characteristics

Fig. 5 shows the relationship between the phase difference of vibration between vibration components A and B and vibration components C and D and the translational movement speed when the actuator was set in a horizontal plane. The input current to vibration components A and B was fixed at 100 mA and that to vibration components C and D was set to 100 or 150 mA. The figure shows that the translational speeds are almost equal when the phase difference is 0 or 180 degrees, which means that the actuator is capable of reciprocating translational movement at a given speed.

Fig. 6 shows the translational movement speed of the actuator in the horizontal plane when the input current to vibration components A and B was fixed at 250 mA and that to vibration components C and D was varied. The ○ and △ marks in the figure show the results when the phase difference of vibration at vibration components A/B and C/D is 0 and 180 degrees, respectively. In the horizontal plane, this actuator is capable of reciprocating movement at approximately the same speed even when the input current is varied.

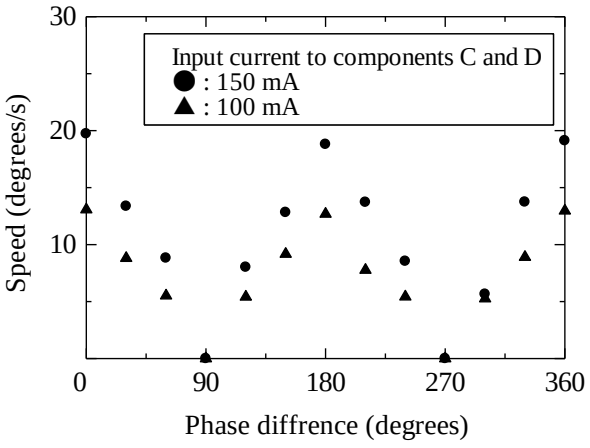

Fig. 5 Relationship between phase difference and Speed (translational movement in horizontal plane)

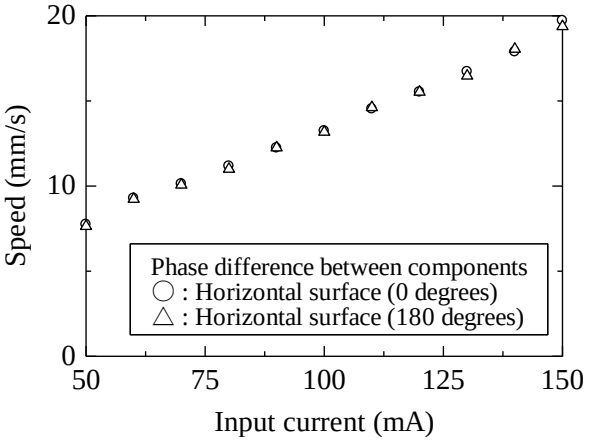

Fig. 6 Relationship between input current and speed (translational movement in horizontal plane)

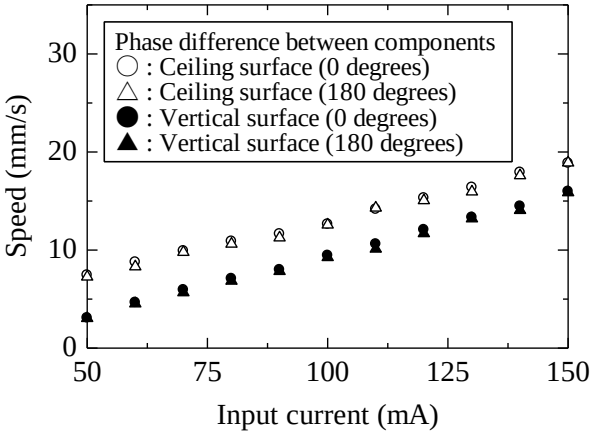

Fig. 7 Relationship between input current and speed (translational movement in ceiling and vertical plane)

Fig. 7 shows the translational movement speed of the actuator when the input current to vibration components A and B was fixed at 250 mA and that to vibration components C and D was varied. The phase difference between the vibration components was set to 0 or 180 degrees. In the figure, the symbols ○ and △ mark the results for the ceiling plane and the symbols ● and ▲ mark the results for the vertical plane. It was confirmed that by changing the phase difference between vibration components A/B and vibration components C/D, the direction of movement could be switched while maintaining almost the same speed. The figure shows that the speed of translational movement is almost the same when the phase difference is 0 or 180 degrees and that the actuator can reciprocate at a given speed in the ceiling and vertical planes. The speed of the actuator increases almost linearly with increasing input current to the electromagnets.

The phase difference between vibration components A/B and vibration components C/D

were set to 0 degrees and measurements were taken.

Fig. 8 shows the relationship between the tilt angle of the surface plate and the translational movement speed of the actuator with the input current to vibration components A and B set to 150 mA and that to vibration components C and D set to 50, 100, or 150 mA. In the figure, -90 degrees indicates vertical downward movement, 0 degrees indicates horizontal movement and 90 degrees indicates vertical upward movement. The dashed line shows the quadratic approximation of the measured values obtained using the least-squares method. As the angle of the steel surface plate is increased, the speed of the actuator gradually decreases.

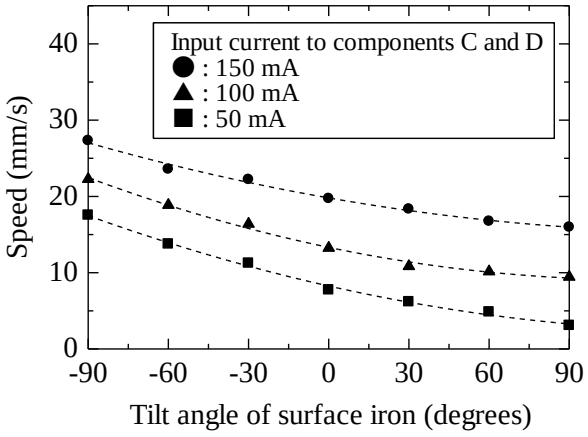

Fig. 8 Relationship between tilt angle and speed (translational movement in the variable plane)

4.3 Load Characteristics

In the following figures, dashed lines show the quadratic approximation of the measured values obtained using the least-squares method.

Fig. 9 shows the relationship between the load mass attached to the actuator and the vertical upward speed, with the input current to vibration components A and B set to 250 mA and that to vibration components C and D set to 160, 180, or 200 mA. The load mass was attached to the acrylic frame of the actuator using a thread. The actuator is capable of vertical upward movement at a speed of 4.4 mm/s while pulling a 130-g mass.

Based on the results obtained in Fig. 9, Fig. 10 shows the relationship between the load mass and the efficiency of the actuator. The efficiency η of this actuator is expressed as follows:

$$\eta\,(\%) = (M_a + M_m)\, v_{up} \times 100 / P_I \qquad (1)$$

where M_a is the total mass of the actuator, M_m is the load mass, v_{up} is the vertical speed, g is the acceleration due to gravity, and P_I is the input power. The maximum efficiency of this actuator was 1.6%,

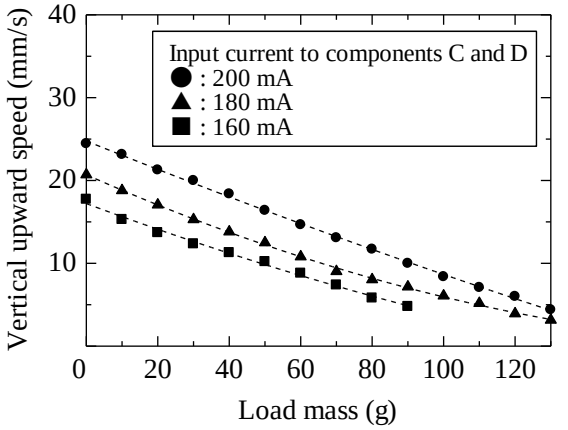

Fig. 9 Relationship between load mass and vertical upward speed (translational movement in vertical plane)

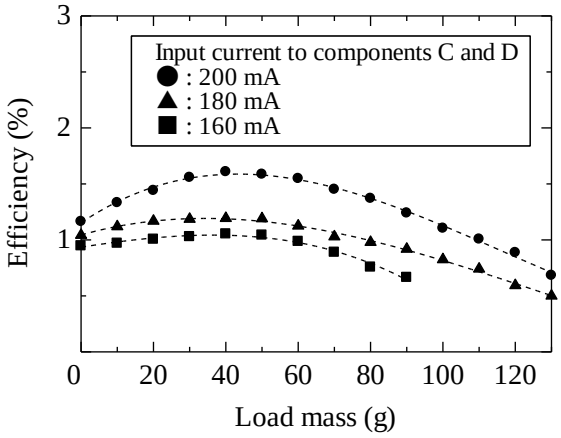

Fig. 10 Relationship between load mass and efficiency (translational movement in the vertical plane)

indicating low-efficiency characteristics. In this paper, multiple vibration components are placed in the frame structure, and the mounting positions of vibration components C and D are increased. The reason is that the large moment acting on the support part of the actuator inhibits the movement of the actuator. The low efficiency of this actuator system is due to the fact that the four vibration components in the system have the same resonant frequency. Since there is vibration interference between the components, methods to reduce these effects will be investigated in the future.

5. MOVEMENT CHARACTERISTICS OF PHASE-CONTROLLED ACTUATOR SYSTEM

5.1 Structure of Actuator System

The prototype actuator described above is only capable of translational reciprocating movement. In

order to control the direction of movement and improve the propulsive characteristics, a new actuator system, in which the previously shown actuators are connected in parallel, is proposed. As shown in Fig. 11, two actuators, A and B, with identical characteristics were fabricated. When both actuators were connected with a stiff plastic material, the actuator system could not move due to increased vibration interference between the vibration components. Therefore, an actuator system was fabricated in which actuators A and B were joined by five pieces of flexible silicone rubber (thickness: 6 mm, width: 15 mm, length: 75 mm), as shown in Fig. 12.

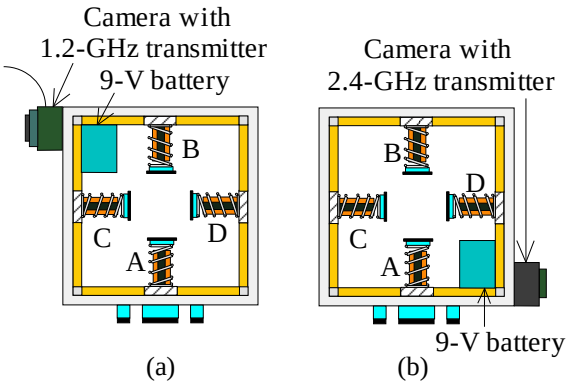

Fig. 11 Structure of two sets of actuators: (a) actuator A and (b) actuator B making up actuator system

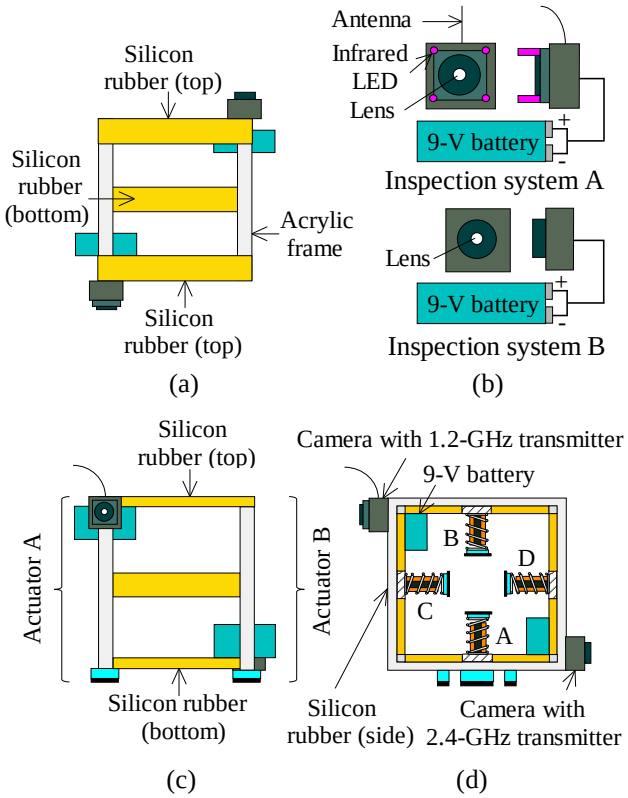

Fig. 12 Structure of actuator system: (a) plan view, (b) inspection system, (c) front view and (d) side view of actuator system connected by silicone rubber

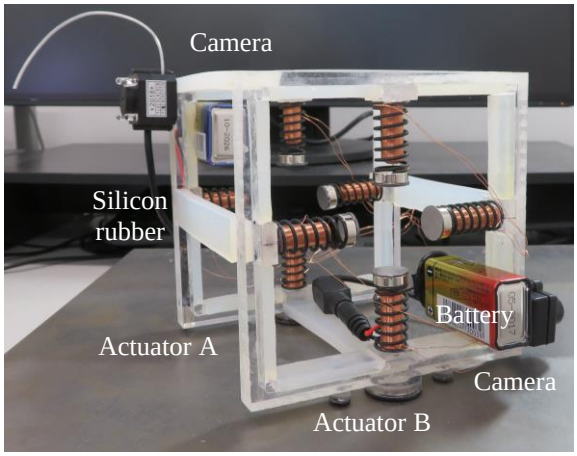

Fig. 13 Photograph of actuator system

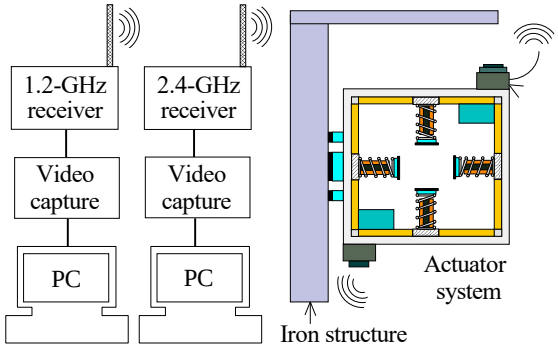

Fig. 14 System capable of inspection inside iron structure (PC: personal computer)

As mentioned above, this actuator has a frame structure for mounting an inspection system. Image signals from small cameras, which are commonly used as inspection devices, are subject to increased resistance and loss of electric power when long cables are used, resulting in degraded image quality. To prevent this, commercially available cables made specifically for image transmission can be used. A thin cable with a diameter of 4 mm has a mass of 230 g per 10 m. Therefore, when two cameras are mounted on the actuator system, an extremely high traction force is required, taking into account the mass of the cables and the friction force.

Considering these issues, two wireless inspection systems (A and B) were attached to the actuator system, as shown in Figs. 11 and 12. The two inspection systems allow visual inspection of the front and rear surfaces of the structure. System A consists of a small camera (with a built-in 1.2-GHz transmitter and four infrared LEDs) and a 9-V battery. System B consists of a small camera (with a built-in 2.4-GHz transmitter) and a 9-V battery. The mass of the small cameras of systems A and B is 8.5 and 10 g, respectively, and the mass of the 9-V battery is 43 g. Fig. 13 shows a photograph of the prototype actuator

system.

As shown in Fig. 14, the actuator system enables visual inspection of iron structures using two receivers, a video capture device, and a personal computer. The prototype actuator system is 110 mm long, 97 mm wide, and 116 mm high, and has a total mass of 354.5 g. The total mass of the system without the two inspection systems is 250 g. Two sets of the experimental apparatus shown in Fig. 4 were prepared to drive the actuator system.

5.2 Principle of Rotation Operation

In this actuator system, two actuators with identical specifications are arranged in parallel. Therefore, the system can be rotated to move to any position. In this actuator system, actuator A is operated and actuator B is stationary, as shown in Fig. 15(a). A moment is generated and applied to the center (fulcrum) of actuator B on the stationary side, allowing the actuator system to rotate counterclockwise. Actuator B is operated as shown in Fig. 15(b). By applying a moment to the fulcrum of actuator A, the actuator system can rotate clockwise. Thus, by driving actuator A or B, the actuator system can rotate in any direction. By combining rotation and translational movement, the actuator system can move in any direction.

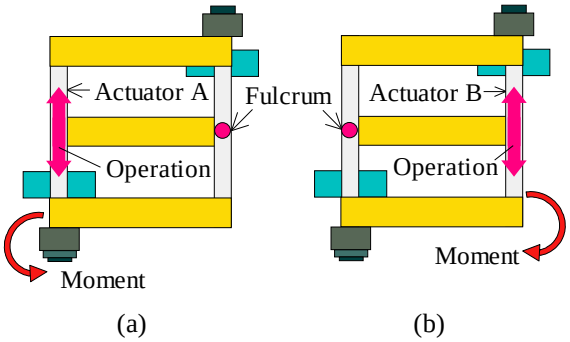

Fig. 15 Principle of turning: (a) counter-clockwise and (b) clockwise direction of actuator system

5.3 Movement Characteristics of Actuator System

The rotational speeds in the prototype actuator system were measured. Fig. 16 shows the relationship between the input current to vibration components C and D and the rotational speed of the system in the horizontal and vertical planes, with the input current to vibration components A and B fixed at 250 mA. In this figure, ○ and ● mark the results when the phase difference between vibration components A/B and C/D is 0 and 180 degrees, respectively, in the horizontal plane, and ▲ and △ mark the results when the phase difference between vibration components A/B and C/D is 0 and 180 degrees, respectively, in the vertical plane. The figure shows that this actuator system can be rotated

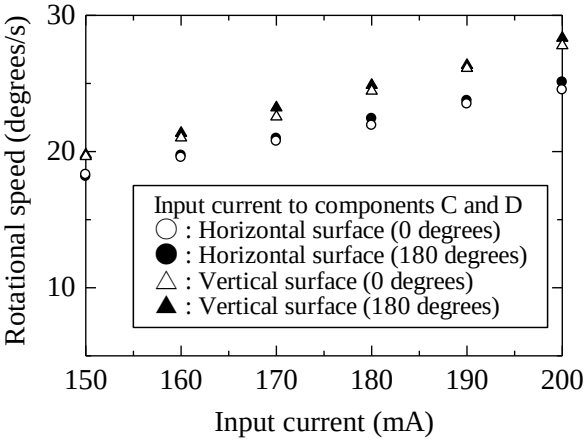

Fig. 16 Relationship between input current and rotational speed (translational movement in horizontal plane)

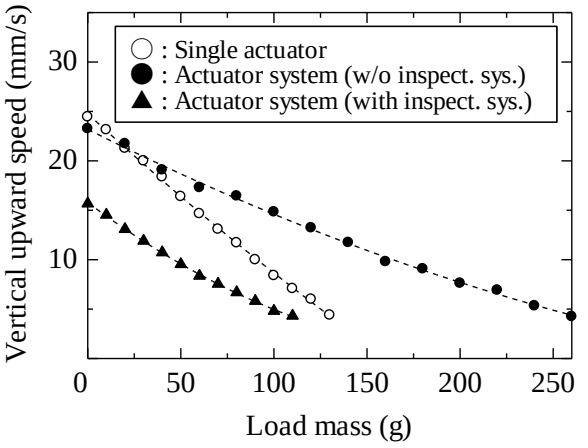

Fig. 17 Relationship between input current and rotational speed (translational movement in vertical plane)

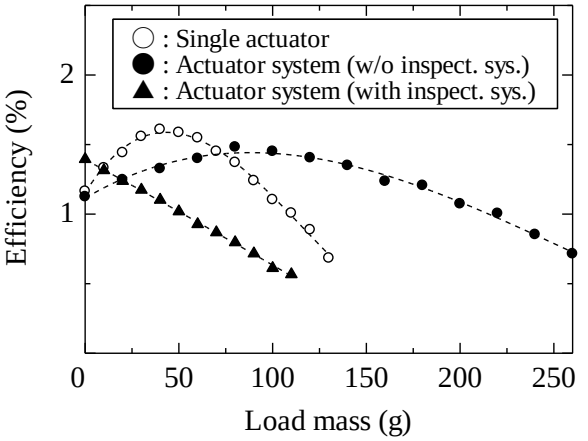

Fig. 18 Relationship between input current and rotational speed (translational movement in vertical plane)

at almost the same rotational speed in both the horizontal and vertical planes.

Fig. 17 shows the relationship between the load mass attached to the system and the vertical upward speed, with the input current to vibration components A and B fixed at 250 mA and the input current to vibration components C and D fixed at 200 mA. In the figure, ○ marks the results for a single actuator, ▲ marks the results for the actuator system with the inspection systems, and ● makes the results for the actuator system without the inspection systems. The figure shows that the vertical upward speed decreases as the load mass increases. The traction force of the actuator system without the inspection systems is twice that of the actuator. The maximum traction force of the actuator system with the two inspection systems was only 110 g (1.1 N).

In this actuator system, the maximum input voltage and current to a single electromagnet are 3.3 V and 0.25 A, respectively. Considering these input values, only eight cables with a diameter of 0.3 mm are required to drive the electromagnets. The mass per 10 m of the eight cables is about 43 g. Since the maximum radio wave range of an inspection system is about 30 m, this actuator system can be used to inspect a structure over long distances.

Based on the results obtained in Fig. 17, Fig. 18 shows the relationship between the load mass and the efficiency of the actuator system and the single actuator. From the figure, the maximum efficiency of the actuator system with inspection system is about 1.4%. Two inspection systems increase the moment in the support part of the actuator system, further reducing its efficiency compared to the single actuator. However, the actuator system with two wireless inspection systems has adequate propulsion characteristics. The operation of inspection system beneficial to bridge inspection was established by an actual machine test.

All results for the actuators and actuator systems prototyped in this study are averaged from data measured three times. Therefore, the driving characteristics of the actuator system presented in this paper are easily reproduced.

This actuator system can operate on iron structures that have some rust and water droplets. Based on the results obtained above, bridge inspections in the field can be performed by carrying one portable power supply, a mobile PC, two two-channel signal generators, and four power amplifiers.

6. CONCLUSIONS

This study proposed a phase-controlled electromagnetic vibration actuator for inspection applications. A prototype of this actuator consisted of four orthogonally arranged vibration components in a square acrylic frame. Tests on the actuator showed that it could move on ceilings and vertical planes. In addition, a prototype actuator system with two inspection systems, which is capable of translational and rotational movement, was developed. The actuator system has a maximum traction force of 1.1 N. It can transmit inspection images wirelessly, allowing inspection inside structures over long distances. The actuator system can move in any direction by combining rotational and translational reciprocating movements. The operation of an industrially useful inspection device was thus established. In addition, this actuator system can also be stuck to the iron bridge by the attraction force of the permanent magnet to monitor its appearance over time.

The propulsion characteristics and efficiency of the actuator system proposed in this paper are low. These are mainly due to small magnetic excitation forces and vibration interference between multiple vibration components. Based on vibration analysis of the frame structure, a new frame should be redesigned to improve the propulsion characteristics, including improvement of the magnetic circuits of vibration components.

7. ACKNOWLEDGMENTS

This work was supported by JSPS KAKENHI Grant Number JP23K03648.

8. REFERENCES

[1] Shen W., Gu J., and Shen Y., Permanent Magnetic System Design for the Wall-Climbing Robot. IEEE International Conference on Mechatronics, 2011, pp. 2078-2083.

[2] Lee G., Parl J., Kim H., and Seo W., Wall Climbing Robots with Track-wheel Mechanism. IEEE International Conference on Machine Learning and Computing, 2011, pp. 334-337.

[3] Suzuki M., and Hirose S., Proposal of Swarm Type Wall Climbing Robot System Anchor Climber and Development of Adhering Mobile Units. The Robotics Society of japan, Vol. 28, No. 5, 2010, pp. 614-623.

[4] Khirade N., Sanghi R., and Tidke D., Magnetic Wall Climbing Devices - A Review. International Conference on Advances in Engineering & Technology, 2024, pp. 55-59.

[5] Kim J., Park S., Kim J., and Lee J., Design and Experimental Implementation of Easily Detachable Permanent Magnet Reluctance Wheel for Wall-Climbing Mobile Robot. Journal of Magnetics, Vol. 15, No. 3, 2010, pp. 128-131.

[6] Kim H., Kim D., Yang H., Lee K., Seo K., Chang D., and Kim J., Development of a wall-climbing robot using a tracked wheel Mechanism. Journal of Mechanical Science and Technology, Vol. 22, 2008, pp. 1490-1498.

[7] Subramanyam A., Mallikarjuna Y., Suneel S., and Kumar L., Design and Development of a Climbing Robot for Several Applications. International Journal of Advanced Computer Technology, Vol. 3, No. 3, 2011, pp. 5-23.
[8] Panich S., Development of a Climbing Robot with Vacuum Attachment Cups. Journal of Computer Science, Vol. 6, No. 10, 2010, pp. 1185-1188.
[9] Wang K., Wang W., Li D., Zong D., Zhang H., Zhang J., and Deng Z., Analysis of Two Vibrating Suction Methods. IEEE International Conference on Robotics and Biomimetics, 2008, pp. 1313-1319.
[10] Wang W., Wang K., Zhang H., and Zhang J., Internal Force Compensating Method for Wall-Climbing Caterpillar Robot. IEEE International Conference on Robotics and Automation, 2010, pp. 2816-2820.
[11] Xu F., Wang X., and Jiang J., Design and Analysis of a Wall-Climbing Robot Based on a Mechanism Utilizing Hook-Like Claws. International Journal of Advanced Robotic Systems, Vol. 9, No. 261, 2012, pp. 1-12.
[12] Funatsu M., Kawasaki Y., Kawasaki S., and Kikuchi k., Development of cm-scale Wall Climbing Hexapod Robot with Claws. International Conference on Design Engineering and Science, 2014, pp. 101-106.
[13] Provancher W., Jensen-Segal S., and Fehlberg M., ROCR: An Energy-Efficient Dynamic Wall-Climbing Robot. IEEE Transaction on Mechatronics, Vol. 16, No. 5, 2011, pp. 897-906.
[14] Hagiwara T., Yamamura Y., Namima Y., Ogami J., and Pengfei L., Production of Crawler Robot with Sub Crawler and Verification of Traversing Ability. 2th International Symposium on Instrumentation Control Artificial Intelligence and Robotics (ICA-SYMP), 2021, pp. 1 - 4.
[15] Kumar S., and Arora M., Design and Application of Crawler Robot. 6th National Conference on Advancements in Simulation and Experimental Techniques in Mechanical Engineering (NCASEme), 2019, pp. 90 - 94.
[16] Tao C., and Liu B., Online Autonomous Motion Control of Communication-Relay UAV with Channel Prediction in Dynamic Urban Environments. Drones, 2024, Vol. 8, No. 12, pp. 1-25.
[17] Rushood M., Rahbar F., Shokri S., Selim S., and Dweiri F., Accelerating Use of Drones and Robotics in Post-Pandemic Project Supply Chain. Drones, Vol. 7, No. 55, 2023, pp. 1 - 9.
[18] Furukawa A., and Jiang M., Estimating Natural Vibration Characteristics of Bridge Cables Based on N4SID Subspace Method. International Journal of GEOMATE, Vol. 26, Issue 113, 2024, pp. 98-106.
[19] Tuleyev A., Omarov Z., Abakanov T., Lapin T., and Tuleyev T., Vibration Test of A High-Rise Monolithic Building. International Journal of GEOMATE, Vol. 25, Issue 109, 2023, pp.149-156.
[20] Furukawa A., Yamada S., and Kobayashi R., Tension Estimation Methods for NIELSEN-LOHSE Bridges using Out-of-Plane and In-Plane Natural Frequencies. International Journal of GEOMATE, Vol.23, Issue 97, 2022, pp.1-11.
[21] Furukawa A., and Goto M., Incorporatiog Poisson Effect into DEM for Enhanced numerical Analysis of Masonry of Structure. International Journal of GEOMATE, Vol. 27, Issue 119, 2024, pp. 1-9.
[22] Urakawa A., Sasaki T., and Cho H., Dynamic Properties of Post-Buckled Shape Memory Alloy and its Application to a Base Isolator for Vertical Vibration. International Journal of GEOMATE, Vol.20, Issue 82, 2021, pp.101-108.
[23] Chen J., Jiang J., Wang K., and Zhang F., Optimal Placement of Actuators for Active Vibration Control Using EER and Genetic Algorithm. 10th IEEE International Conference on Mechanical and Aerospace Engineering (ICMAE), 2019, pp. 459- 453.
[24] Li J., Xue Y., Li F., and Narita Y., Active Vibration Control of Functionally Graded Piezoelectric Material Plate. Composite Structures, Vol. 207, No. 1, 2019, pp. 509-518.
[25] Yaguchi H., A New Type of Electromagnetically Propelled Vibration Actuator for Appearance Inspection of Iron Structure. International Journal of GEOMATE, Vol. 20, No. 77, 2021, pp. 69 - 76.
[26] Yaguchi H., and Sato R., A New Type of Electromagnetic Vibration Actuator Capable of Combined Linear and Rotational Motion. International Journal of GEOMATE, Vol. 26, No. 117, 2024, pp. 68 - 77.